Supporting information for

Enhanced Photoacoustic Detection of Heparin in Whole Blood *via* Melanin Nanocapsules Carrying Molecular Agents

Wonjun Yim, Kathryn Takemura, Jiajing Zhou, Jingcheng Zhou, Zhicheng Jin, Raina M. Borum, Ming Xu, Yong Cheng, Tengyu He, William Penny, Bill R. Miller III, and Jesse V. Jokerst.

Correspondence to: jjokerst@eng.ucsd.edu

This PDF file includes:

- Materials
- Methods
- Figure S1 to S32
- Table S1
- References
- Descriptions for Movie S1 and S2

Other Supplementary Materials for this manuscript include the following:

- Movie S1 and S2

Materials and Methods

Materials

Benzene-1,4-dithiol (BDT, ≥99%), tannic acid (TA, ACS reagent), sodium dodecyl sulfate (SDS, ≥99%), bicine (≥99%), dopamine hydrochloride (DA, ≥98%), azure A chloride (AA, ≥70%), nile blue A (NB, ≥70%), neutral red (NR, ≥90%), *N,N*–dimethylformamide (DMF), hydrochloric acid (HCl, 36.5–38.0%), sodium hydroxide (NaOH, ≥98%), triton X-100 (BioXtra), dimethyl sulfoxide (DMSO), tween-20 (BioXtra, viscous liquid), calcium chloride solution ($CaCl_2$, 1M), urea (99.0–100.5%), sodium chloride (NaCl, ≥99.5%), chondroitin sulfate, sodium chloride, bovine serum albumin (BSA, ≥95%), hemoglobin powder (Hgb), poly(sodium-4-strynesulfornate) (PSS, M_w ~70,000), Dulbecco's phosphate buffered saline (DPBS), human serum, and protamine sulfate salt from salmon (grade I-A) were purchased from Sigma-Aldrich. Methoxyl poly(ethylene glycol) (PEG) thiol (HS-mPEG, M_w 5k Da) was purchased from Nanocs. Thrombin powder was purchased from Roche. Methylene blue was purchased from Fisher scientific. Dulbecco's modified Eagle's medium (DMEM) was purchased from Thermo Fisher. Heparin (sodium injection at 5,000 and 10,000 United States Pharmacopeia (USP) U/mL) was purchased from SAGENT pharmaceuticals. Carbon/Formvar grids (300 mesh) were purchased from Ted Pella, Inc. Laboratory polyethylene tubing (OD: 1.27 mm, ID: 0.85 mm) was purchased from Harvard apparatus for photoacoustic (PA) measurements. Activated partial thromboplastin time (aPTT) agents were purchased from Diagnostica Stago, NJ. All chemical reagents were freshly prepared for immediate use in each experiment.

Human blood sample preparation, aPTT assay, hemolysis, and specificity test with different biological species.

All work with human subjects was done in accordance with IRB guidelines and approval. All subjects gave informed consent. Whole human blood was collected in citrate tubes from a healthy donor according to the institutional guidelines and stored at 2 ˚C. For PA imaging, 50 μL samples were treated with 50 μL heparin (0–4 U/mL) and imaged within 1 h. To determine the correlation between PA intensity and blood clotting time, poor human plasma that included heparin with the concentration of 0, 0.2, 0.4, 0.6, 0.8, and 1 U/mL was used for aPTT analysis. Blood clotting times were measured in triplicate with an ST4 semi-automated mechanical coagulation instrument (Diagnostica Stago, NJ). Briefly, 50 μL of aPTT reagent was added to 50 μL of citrated plasma and incubated at 37 ˚C with stirring magnetic ball for 5 min. Then, 50 μL of 25 mM $CaCl_2$ was injected to initiate blood clotting. The time required for blood clot was calculated in seconds. For hemolysis analysis, whole human blood cells were incubated with different concentrations of samples (*e.g.,* PNC@MB, PNC@AA, PNC@NB, and PNC) for 4 h. The DPBS and deionized water were used as negative and positive controls, respectively. Then the samples were centrifuged at 4,000 rpm, and the supernatant were collected for the absorbance measurement. For specificity test, PNC@NB was incubated with different biological conditions (*e.g.,* water, heparin, BSA, Hgb,

human pooled plasma (55%), thrombin, DMEM, PSS, relevant ions (*e.g.,* Cl^-, Ca^{2+}), and heparin analogue (*e.g.,* chondroitin sulfate) at the same mass concentration (2 μg/mL)). After 1h, samples were imaged three times independently.

Clinical sample collection

All work with human subjects was done in accordance with institutional review board (IRB) guidelines and approval of UCSD (#180923) and San Diego Veterans Administration hospital (#H170005). All subjects gave informed consent. Clinical samples were collected from 17 patients undergoing invasive clinical cardiac procedures that need anticoagulation with high dose i.v. heparin. 2–5 mL of each clinical sample was collected in parallel with the specimens obtained for the activated clotting time (ACT) from the baseline prior to heparin infusion to the end of heparin infusion for the maintenance of the anticoagulation. The samples were collected at different points of heparin infusion until reaching steady-state anticoagulation (> ACT of 470 s). Then, plasma of each sample was separated and stored at −80 ˚C. The amount of heparin infused in parallel with ACT value was recorded for comparison to the photoacoustic technique. All samples were thawed at 37 ˚C and studied within 12 h of thawing. 50 μL of PNC@NB reacted with 100 μL of each clinical specimen. After 15 min of reaction, the samples were placed into polyethylene tubes (~2 cm long) and imaged with a customized holder.

Surface area calculation

Surface area of PDA nanoparticle and PNC was calculated using the diameter of PDA nanoparticle (60 nm), outer and inner diameter of PNC (80 nm and 40 nm) based on the mathematical formula (πr^2). Fifty nanoparticles were used to calibrate the diameters of PNC and PDA nanoparticle.

Limit of detection calculation

The limit of detection (LoD) was calculated using the limit of blank (LoB).[1] The LoB is the highest signal generated from a sample that contains no analyte. It can be calculated by using the mean and standard deviation (SD) of a blank sample.

$$LoB = mean_{blank} + 1.645(SD_{blank})$$

LoD is the lowest analyte concentration that can be reliably distinguished from the LoB. LoD is calculated by using the LoB and the standard deviation of the sample. The LoD indicates an analyte concentration in which 95% of measured samples are readily distinguished from the LoB while remaining 5% can contain no analyte.

$$LoD = LoB + 1.645(SD_{low\ concentration\ sample})$$

In our experiment, the LoB and LoD were calculated from Figure 4b and Figure S29 using 0 U/mL, 0.1 U/mL (in water), and 0.2 U/mL (in whole human blood).

Loading capacity calculation

Loading capacity of dye-loaded PNCs was calculated using supernatants. The dye-loaded PNCs were centrifuged four times, and the supernatants were saved for absorbance measurement to calculate the amounts of dyes loaded in PNCs. The amounts of free dyes in the supernatants were determined by measuring the absorbance of the supernatant. Then, the amounts of dye loaded in PNCs were calculated by using the absorbance of total free dye used for the reaction and the supernatants obtained from each wash.

Data analysis

PA images were analyzed using ImageJ software (Bethesda, USA).[2] Images were changed to 8-bit images and analyzed with region of interest (ROI) by using integrated density function in ImageJ software. Average value, standard deviation, and linear regression were calculated using prism and origin software.

General characterization

1. Scanning electron microscopy (SEM) images were acquired using a FEI Apreo operating at a voltage of 10 kV and a current of 0.10 nA.
2. Transmission electron microscopy (TEM) images were obtained using a JEOL JEM-1400 Plus operating at 80 kV. TEM images were taken using a Gatan 4k digital camera, and TEM images were processed using ImageJ software (Bethesda, USA).[2] Electron-dispersive X-ray spectroscopy (EDX) were examined using a Thermo Fisher Talos 200X operating at 200 kV.
3. Hydrodynamic size and zeta potential were calculated using dynamic light scattering (DLS) with a Malvern Instrument Zetasizer ZS 90.
4. Absorbance and fluorescence spectra were measuring using a BioTek Synergy H1 plate reader. Samples were measured at the 150 μL scale in 96-well plates. Absorbance was collected from 400 to 900 nm with a step size of 2 nm. Fluorescence emission scans were collected with an excitation wavelength of 600 nm with a step size of 2 nm.
5. Nanoparticle tracking analysis (NTA) measurement was performed using a ViewSizer 3000 (Horiba Scientific, CA, USA).[3] The temperature was controlled at 27 ˚C during the measurement. Automated noise analysis is used to determine the optimal wavelength for representing each nanoparticle. 8-bit composite video is generated for analysis, and 15 videos were recorded at a framerate of 30 fps for 10 s (300 frames for seconds). A quartz cuvette cell with a minimum volume of 0.8 mL was used for measurement. For the measurement, 50 μL of each sample was diluted in 2 mL of Millipore water. NTA measurement also can image nanoparticles with three lasers with different wavelengths (*e.g.,* red: 630 nm, green: 520 nm, and blue: 445 nm). Red laser is used to scatter large nanoparticles (300–500 nm), while blue laser is used to scatter small nanoparticles (20–200 nm). In this study, both PNC and PBDT@PDA nanoparticles were imaged using blue laser. ImageJ was used to change the color of PBDT–TA@PDA nanoparticle from blue to pink for particle comparison.

6. PA imaging was acquired using a Vevo 2100 LAZR (Visual Sonics, USA) with a 21 MHz transducer (LZ-250). 20 µL samples were loaded into polyethylene tubes and fixed within a 3D printed holder. The samples were aligned at a depth of 1 cm from the transducer. The laser was optimized and calibrated before the measurement. An installed motor with the step size of 0.054 mm was used to acquire 3D images. PA spectra were measured from 680 to 970 nm with the step size of 2 nm.

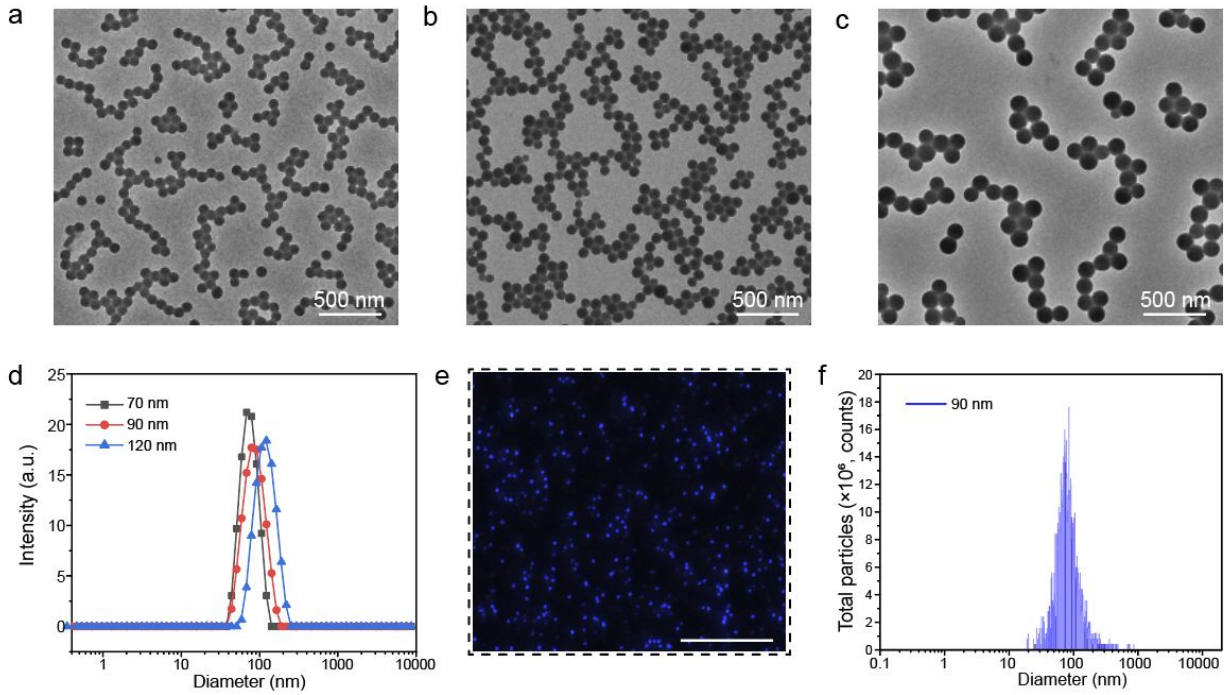

Figure S1. PBDT–TA core nanoparticles.

TEM image of PBDT–TA nanoparticles with diameters of (**a)** 70 nm, (**b)** 90 nm, and (**c)** 120 nm. The size is readily tunable by adjusting the amount of BDT used for the reaction. The ratio of BDT and TA was 0.3:1 (70 nm), 0:5 (90 nm), and 1:1 (120 nm). **d** DLS data shows that PBDT–TA nanoparticles were highly uniform and monodispersed (PDI < 0.1). **e** NTA images of PBDT–TA nanoparticles. The scale bar represents 10 µm. **f** Size distribution of PBDT–TA nanoparticles with the average diameter of 90 nm measured by NTA technique.

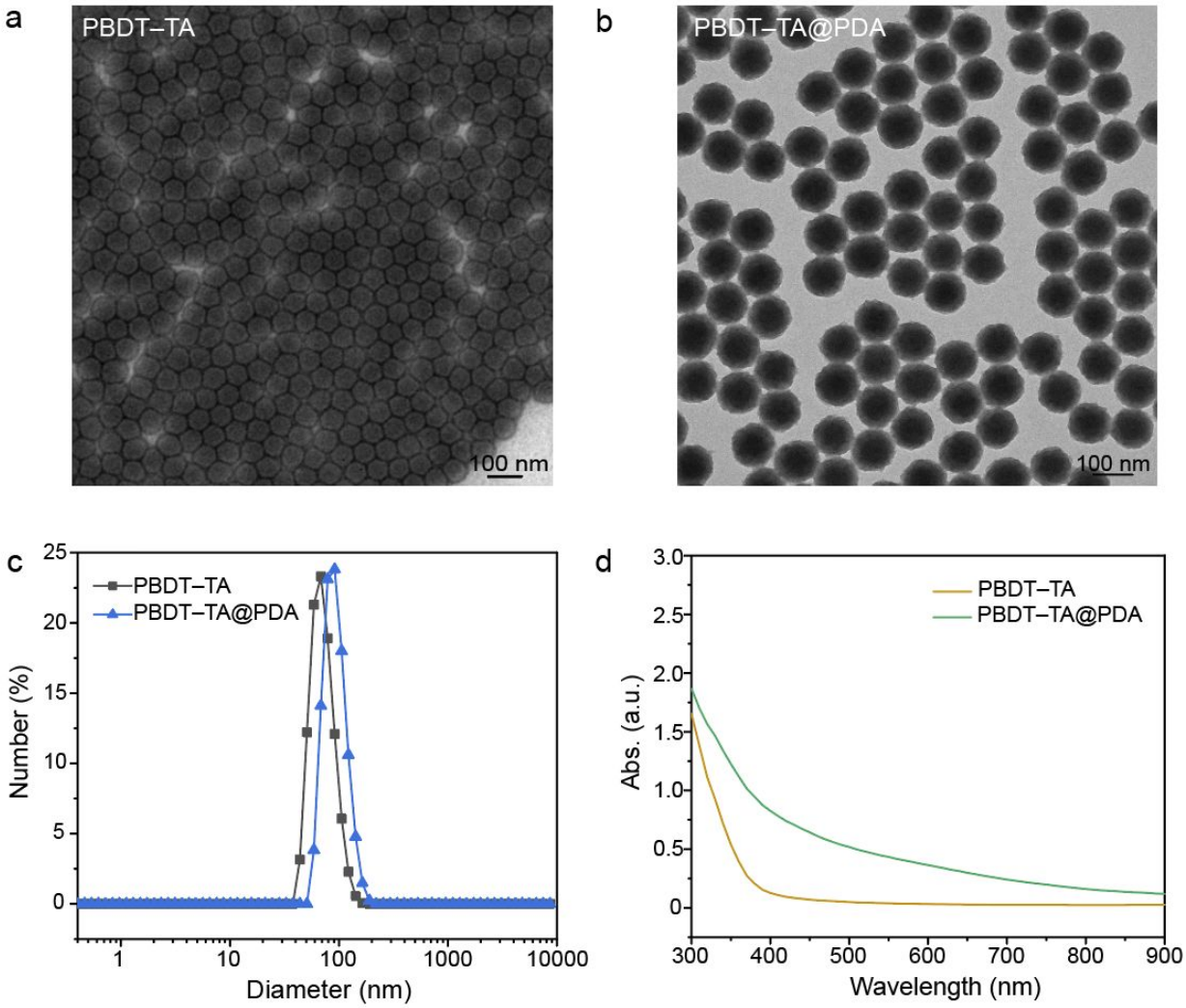

Figure S2. Characterization of core–shell nanoparticles.

TEM image of (**a**) PBDT–TA core and (**b**) PBDT–TA@PDA core–shell nanoparticles. **c** DLS data shows that the size of PBDT–TA nanoparticles increased after PDA coating. **d** UV–vis–NIR spectra of PBDT–TA and PBDT–TA@PDA nanoparticles.

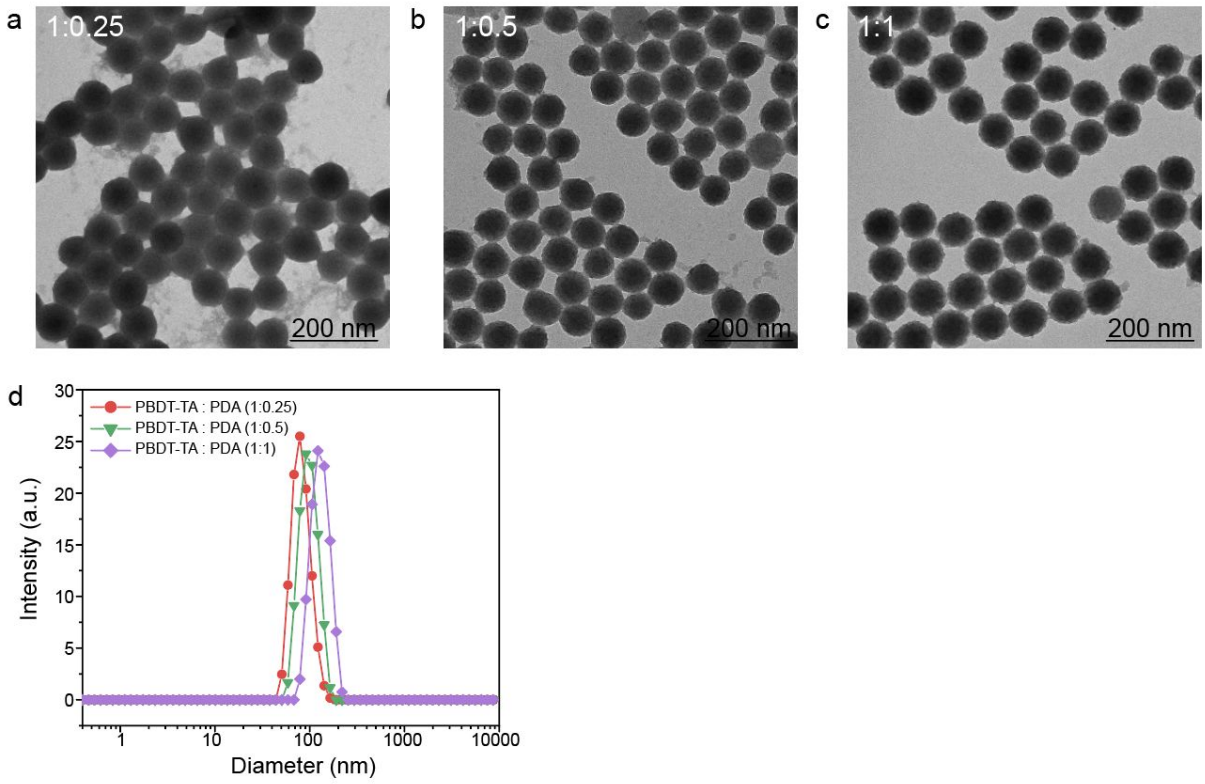

Figure S3. PBDT–TA@PDAs with different PDA thicknesses.
PDA thickness is tunable by adding different amounts of dopamine at the fixed concentration of PBDT–TA nanoparticle. 1:0, 1:0.25, 1:0.5, and 1:1 indicate the ratio of fixed concentration of PBDT–TA to dopamine concentrations. TEM image with different PDA shell thicknesses: (**a**) 5 nm, (**b**) 10 nm, and (**c**) 30 nm. **d** DLS data shows that the particle size increased as adding more dopamine. The diameter of the core–shell particle was 75.2 nm ± 6.2 nm, 83.5 nm ± 7.7 nm, and 101.2 ± 3.7 nm, respectively. The average and standard deviation were calculated from 30 core–shell nanoparticles.

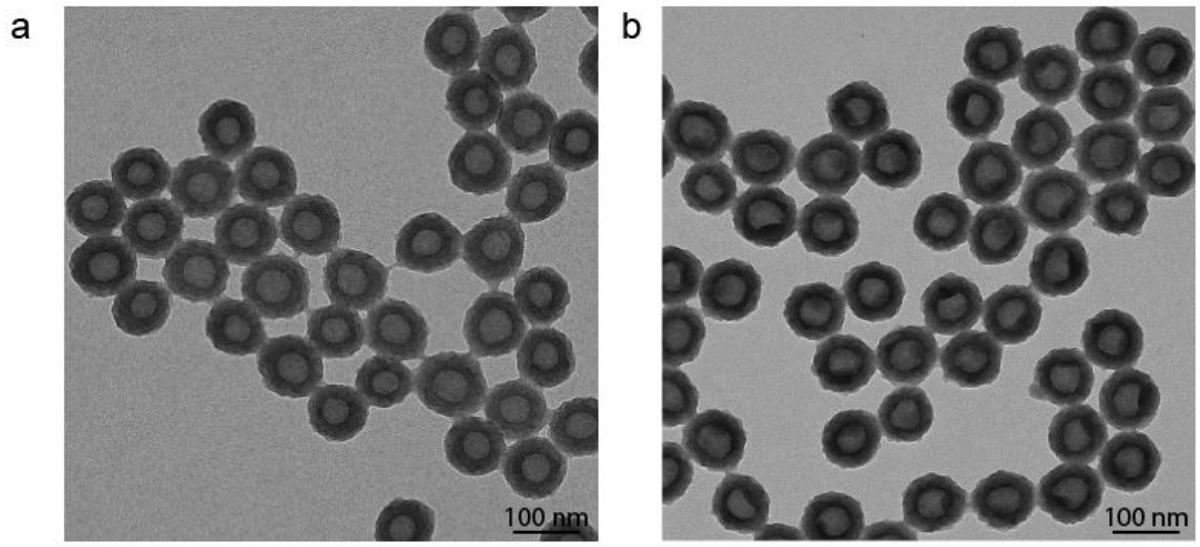

Figure S4. Monodisperse PNC.
TEM image of robust PNC after (**a**) 1 h, and (**b**) 12 h of PBDT–TA@PDA incubation in DMF. PBDT–TA templates are easily disassembled in organic solvent due to the breakage of π–π stacking.[4]

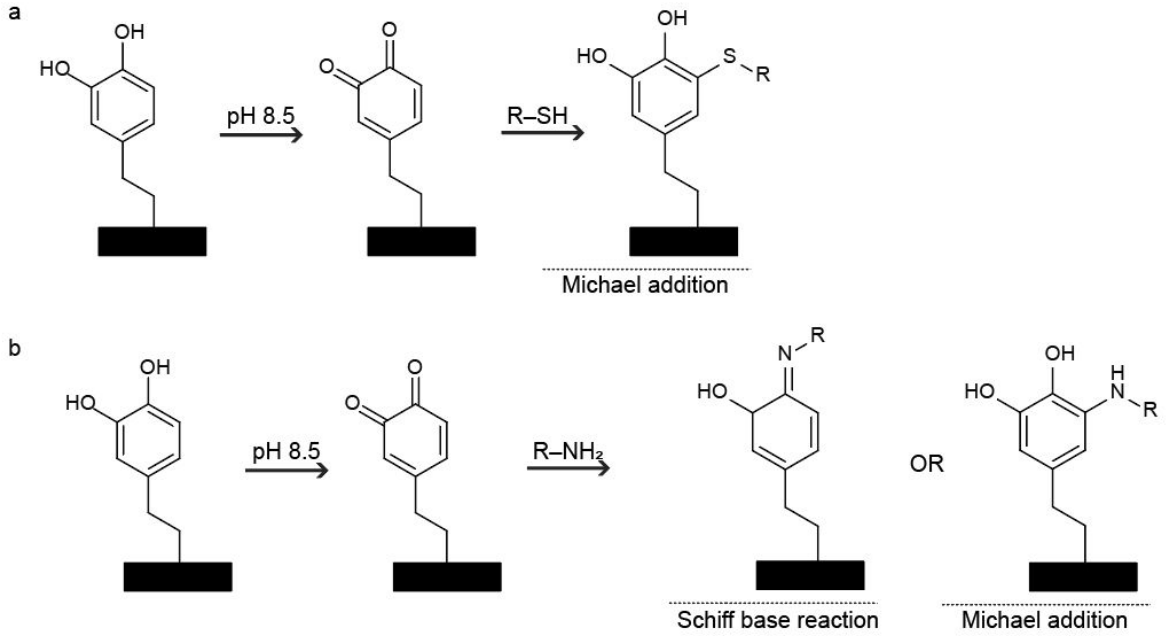

Figure S5. Michael addition and Schiff base reactions of PDA.
Schematic illustration of Michael addition and Schiff base reactions of (**a**) thiol or (**b**) amine ligands with reactive dopamine quinone.[5] It is known that thiol ligand can interact with catechol groups in PDA based on covalent bonding-mediated Michael addition.

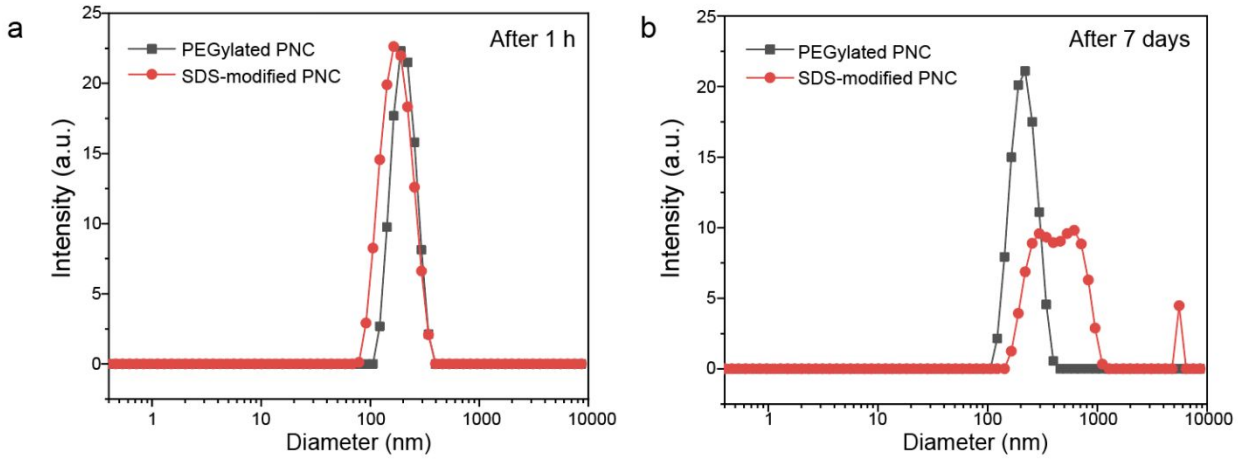

Figure S6. Colloidal stability of PEGylated PNC.
PEGylated PNC successfully loaded free MB dye and maintained colloidal stability as observed by DLS data of after (**a**) 1 h and (**b**) 7 days of loading free MB dyes. However, SDS-modified PNC showed particle aggregation after 7 days of loading free MB dyes.

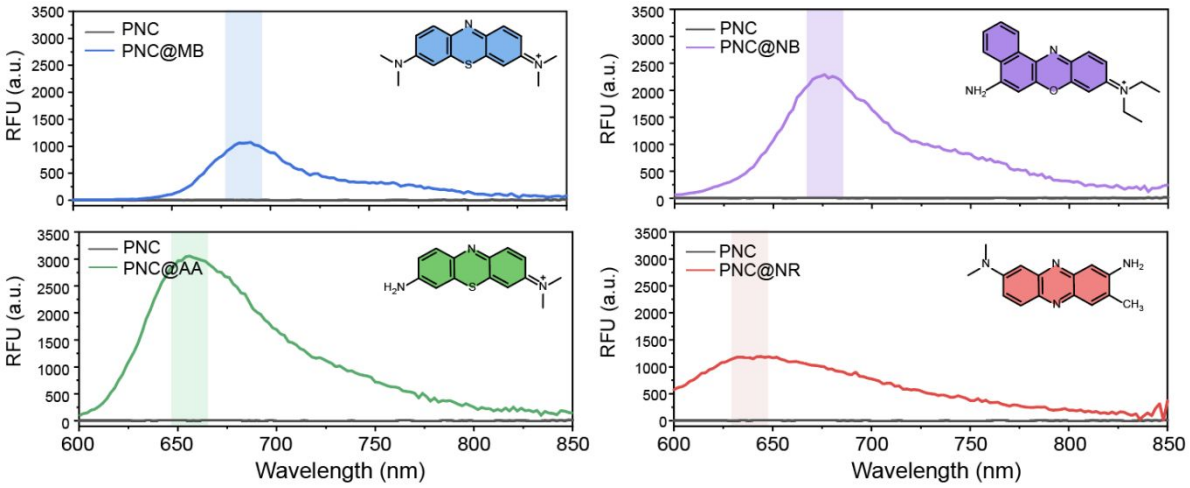

Figure S7. Fluorescence of dye-loaded PNC.
After loading free molecular dyes (*e.g.,* MB, AA, NR, and NB) in PNCs, dye-loaded PNCs emitted fluorescence, while PNC alone had no fluorescence. Excitation wavelength of 600 nm was used for the measurement.

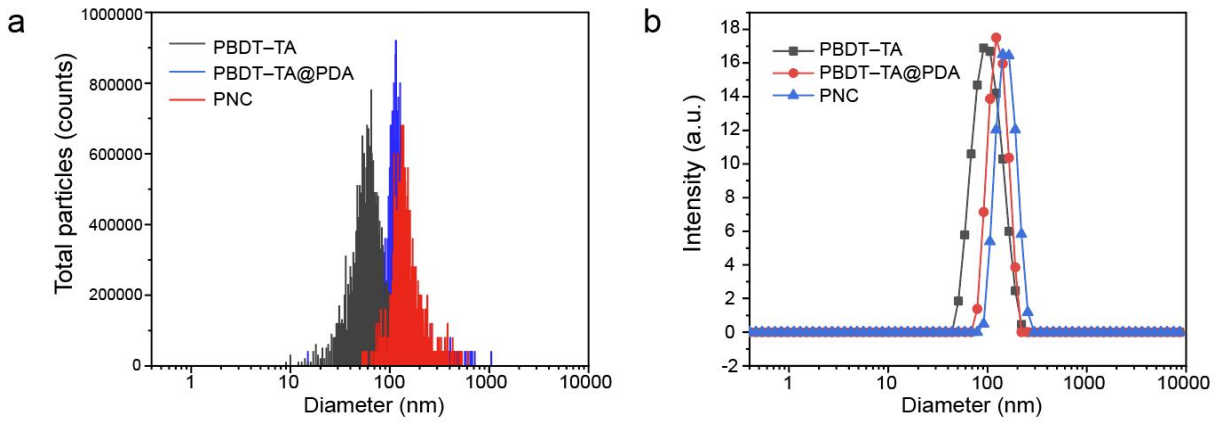

Figure S8. Nanoparticle tracking analysis of PNC.
NTA technique was used to calibrate particle concentration and size distribution of PBDT–TA, PBDT–TA@PDA, and PNC. Size distribution of PBDT–TA, PBDT–TA@PDA, and PNC measured by NTA technique (**a**) was matched with DLS data (**b**). The average sizes of PBDT–TA, PBDT–TA@PDA, and PNC were 72 nm, 133 nm, and 161 nm, respectively.

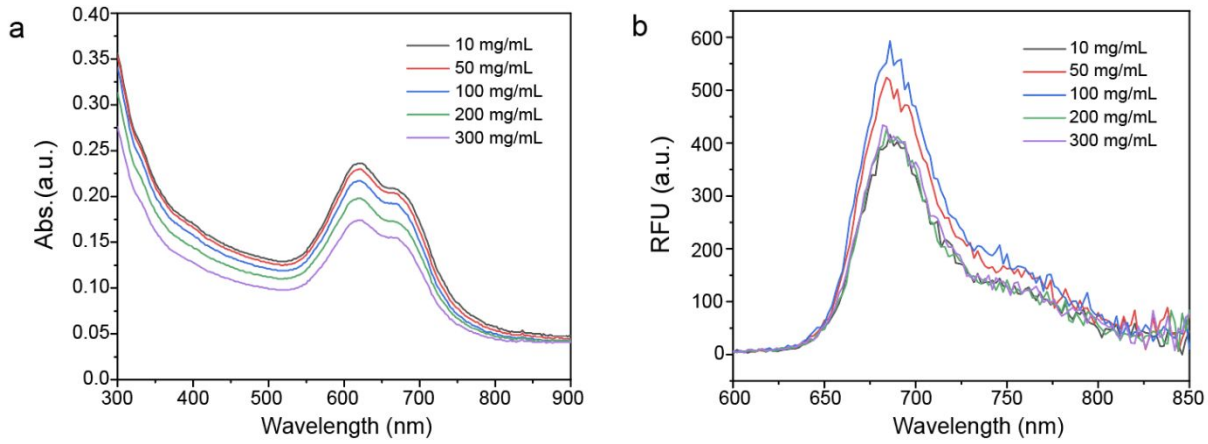

Figure S9. PNC modified with different concentrations of HS-mPEG.
PNC modified with different concentration of HS-mPEG (*e.g.,* 10, 50, 100, 200, and 300 mL of 0.5 wt% HS-mPEG as a starting concentration for PEGylation) to load free MB dye. After PEGylation, samples were centrifuged twice to remove excess of HS-mPEG. **a** UV–vis–NIR spectra of PNC@MB that modified with different concentration of HS-mPEG. Less PEGylated PNC (*e.g.,* 10 mL) had higher absorption peak than more PEGylated PNC (*e.g.,* 300 mL) after loading free MB dye. **b** There was self-quenching of fluorescence on PNC@MB when free MB dyes were over-loaded in PNC.

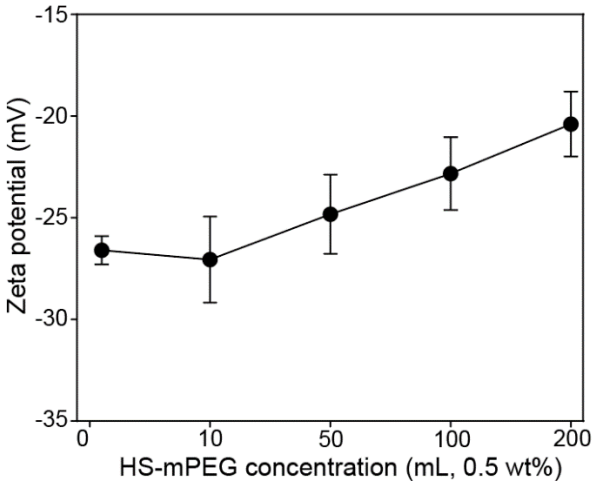

Figure S10. Surface charge of PEGylated PNC.
Zeta potential of PNC modified with different amounts of SH-mPEG (*e.g.,* 0, 10, 50, 100, and 200 as a starting concentration for PEGylation). The surface charge of PNC increased as more SH-mPEG conjugated on the PNC surface. This is because the neutral PEG chain on the exterior layer of PNC can shield the terminal hydroxyl group in PDA, thus reducing the net negative charge of PNC for capturing positively charged dyes. The error bars represent the standard deviation of three separate measurements.

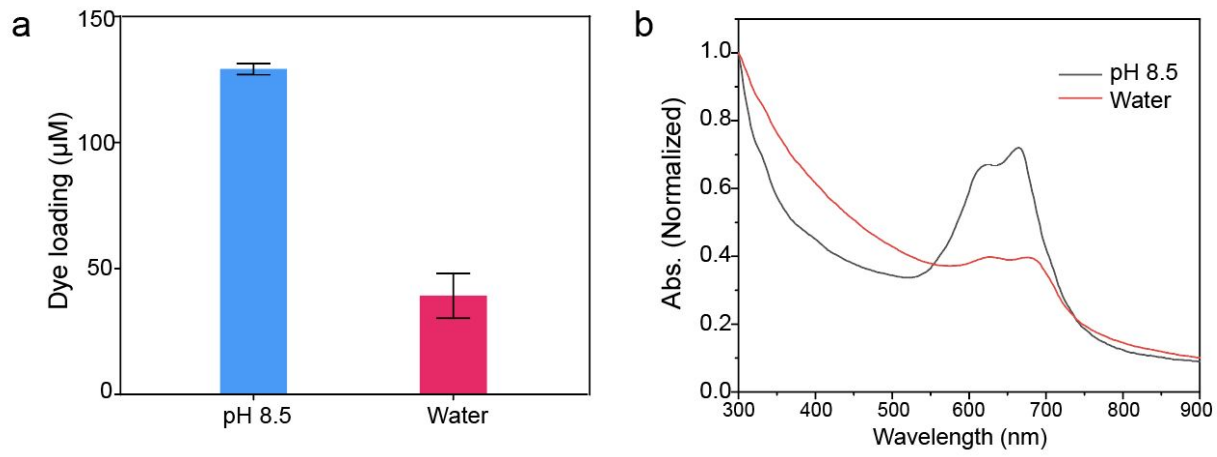

Figure S11. Loading free dyes in PNC in a basic condition.
a Amounts of MB dyes loaded in PEGylated PNCs under basic condition and water. The error bars represent the standard deviation of three separate measurements. **b** UV–vis–NIR spectra of PNC that loaded MB dyes under pH 8.5 and water. PNC@MB that loaded free MB dyes under the basic condition showed two-fold higher absorption peak at 666 nm than PNC@MB that loaded free MB dyes under the water.

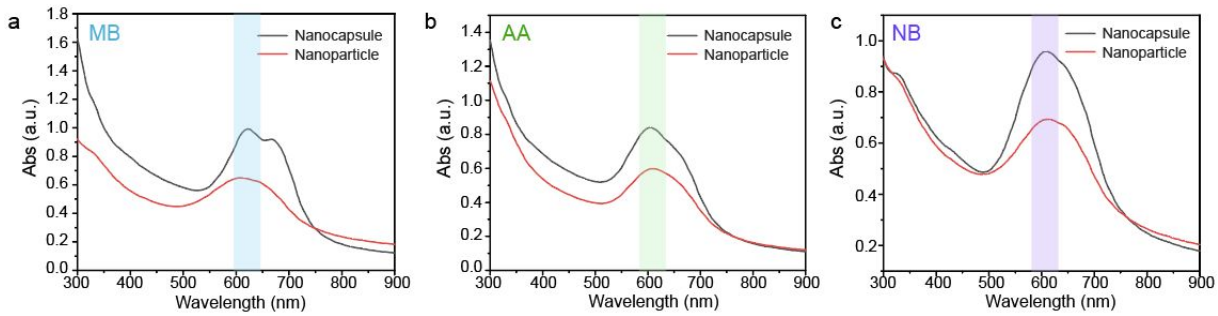

Figure S12. Absorbance of dye-loaded PNC and PDA nanoparticles.
UV–vis–NIR spectra of (**a**) MB, (**b**) AA, and (**c**) NB-loaded PNCs compared to dye-loaded PDA nanoparticles. Dye-loaded PNCs showed at least 1.3-fold higher absorption peak than dye-loaded PDA nanoparticles. These results indicate that hollow PDA structure can load more free dye than PDA nanoparticles due to the increased surface area.

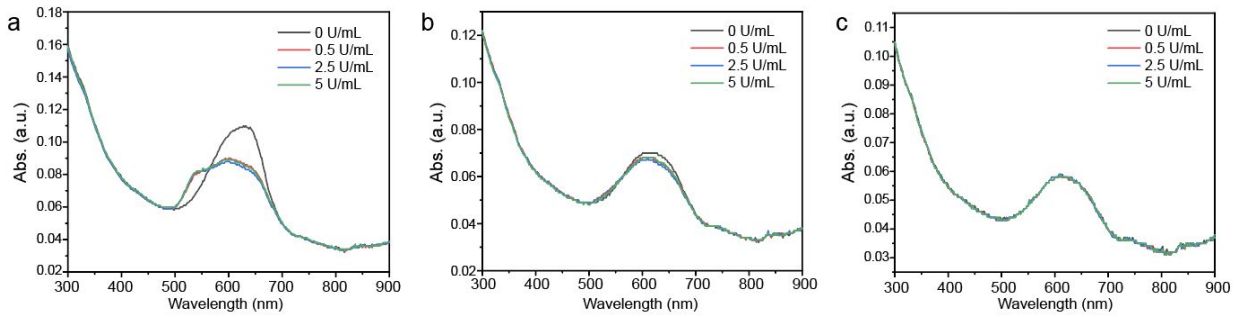

Figure S13. Ruling out the interference of free dye in heparin-dye interactions.
After incorporating free MB dyes into PNC, we conducted four rounds of centrifugations to remove free MB dyes in supernatant. UV–vis–NIR spectra of interaction between heparin and the collected supernatant from (**a**) first (**b**) second, and (**c**) third-times centrifugations. These results indicate that there was negligible involvement of free MB dyes upon heparin interaction after three times of centrifugation. Dye-loaded PNCs were purified by four rounds of centrifugations to remove free molecular dyes in the supernatant.

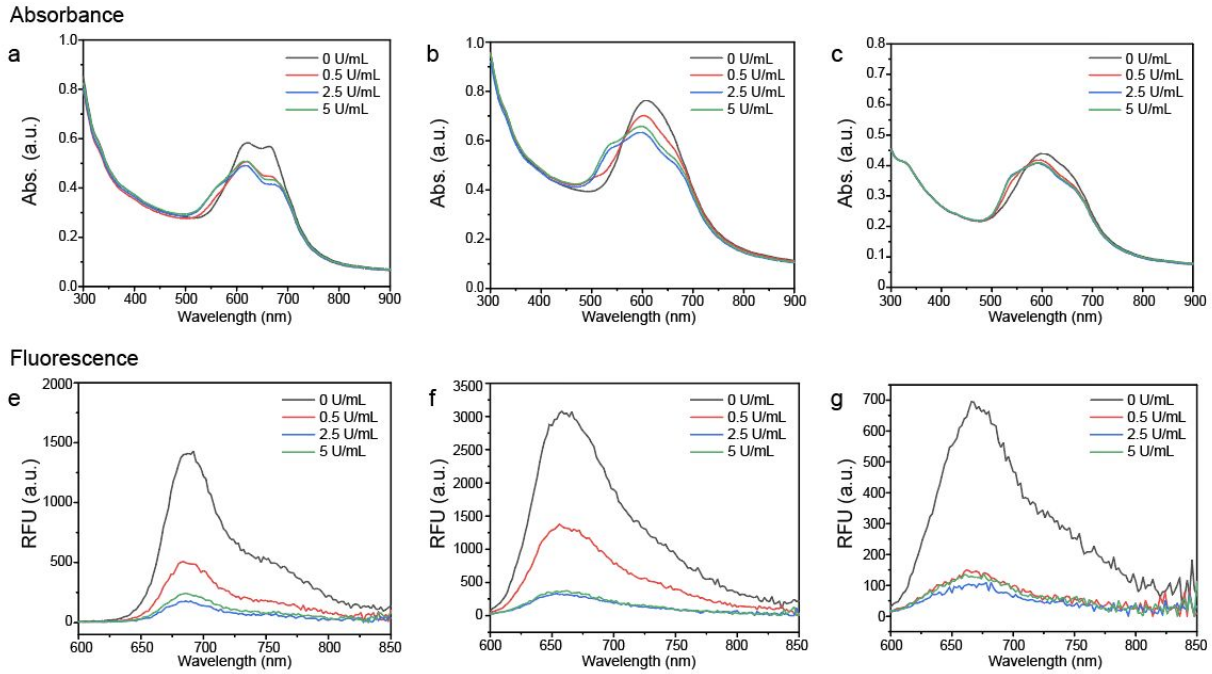

Figure S14. Optical changes of dye-loaded PNC.
Absorbance and fluorescence changes of PNC@MB (**a**, **e**), PNC@AA (**b**, **f**), and PNC@NB (**c**, **g**) were observed after heparin interactions from 0 to 5 U/mL. After heparin interactions, the absorption peaks of PNC@MB, PNC@AA, and PNC@NB decreased and blue-shifted. Likewise, the fluorescence of PNC@MB, PNC@AA, and PNC@NB largely attenuated.

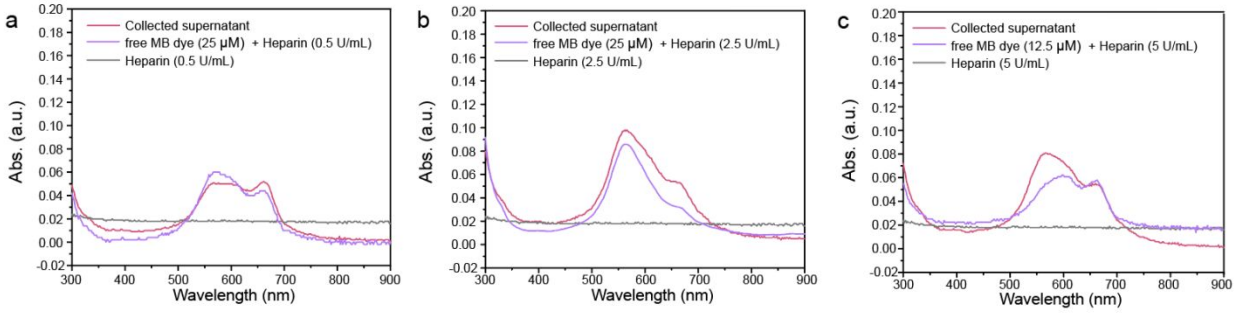

Figure S15. Release of the loaded MB dye in PNC.
After heparin interaction, PNC@MB were centrifuged down, and the supernatant was collected to measure the absorbance. UV–vis–NIR spectra shows that the absorbance obtained from the collected supernatant at heparin concentration of (**a**) 0.5 U/mL, (**b**) 2.5 U/mL, and (**c**) 5 U/mL was matched with the absorbance of free MB dye–heparin interaction at the same heparin concentration. These results validate that the loaded dyes in PNCs disassembled during heparin interaction.

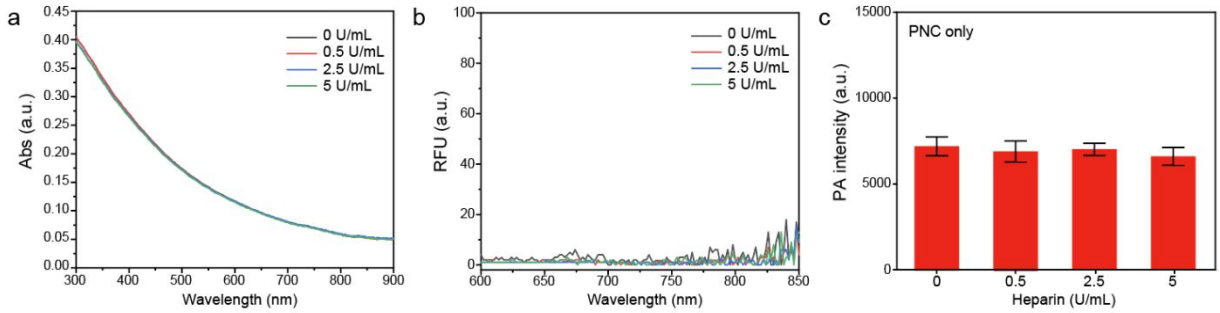

Figure S16. No interaction between PNC alone and heparin.
a Absorbance and (**b**) fluorescence of PNC when interacting with heparin concentration from 0.5 to 5 U/mL. UV–vis–NIR spectra shows that there was no change of absorbance and fluorescence of PNC. **c** Importantly, there was no change of PA intensity of PNC after heparin interactions. These results indicate that the loaded dye in PNC is a function of heparin interaction. The error bars represent the standard deviation of five regions of interest.

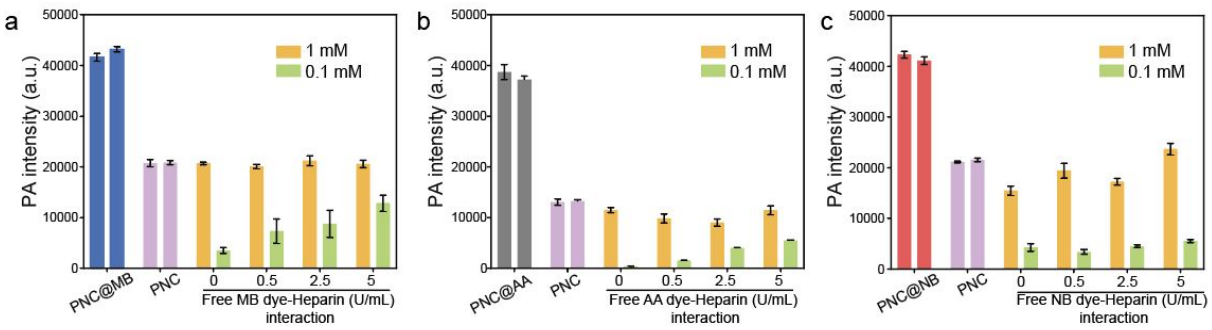

Figure S17. PA intensity comparison.
PA intensities of (**a**) PNC@MB, (**b**) PNC@AA, and (**c**) PNC@NB were compared to free dye–heparin interactions. 1 mM and 0.1 mM of each free dyes interacted with heparin concentration from 0.5 to 5 U/mL, and measured PA signal for the comparison. These results indicate that dye-loaded PNCs generated higher PA signal than free dye–heparin interaction. Blue, gray, and red bars represent PA signal of PNC@MB, PNC@AA, and PNC@NB, respectively. Purple bar represents PA signal of PNC alone. The error bars represent the standard deviation of five regions of interest.

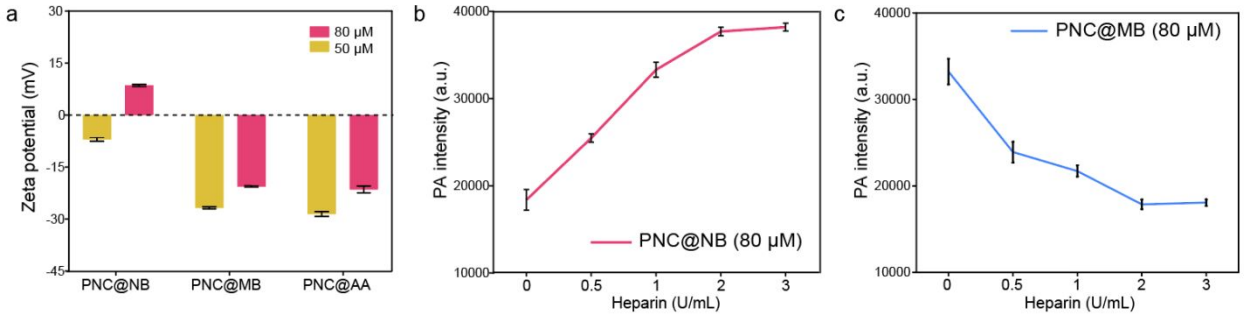

Figure S18. Surface charge-dependent PA signal.
a Zeta potential of PNC@MB, PNC@AA, and PNC@NB that loaded 50 or 80 μM dyes in PNC. PNC@NB which loaded 80 μM showed positively charged surface (+8.5 mV), while PNC@MB (–20.6 mV) and PNC@AA (–21.5 mV) showed negatively charged surface. The error bars represent the standard deviation of three separate measurements. PA signal of (**b**) PNC@NB and (**c**) PNC@MB that loaded 80 μM dye after heparin interaction from 0 to 3 U/mL. PA intensity of positively charged PNC@NB increased after heparin interactions, while PA signal of negatively charged PNC@MB decreased. The error bars represent the standard deviation of five regions of interest.

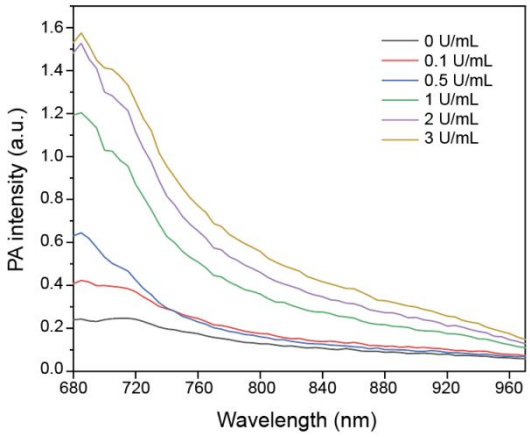

Figure S19. PA spectra of PNC@NB.
PNC@NB showed increased PA signal of PNC@NB from 650 nm to 970 nm wavelength after heparin interactions with heparin concentration from 0 to 3 U/mL.

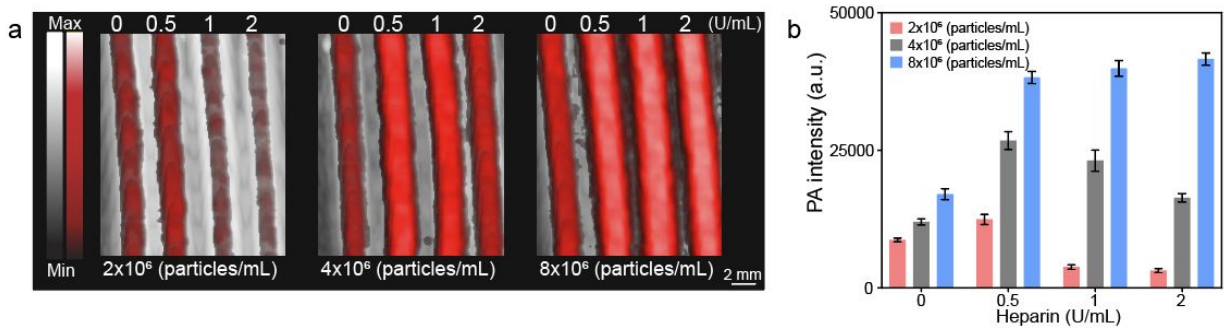

Figure S20. Concentration-dependent PA signal.
a PA image and (**b**) PA intensity of PNC@NB with different particle concentrations (*e.g.,* 2, 4, and 8×10^6 particles/mL) that interacted with heparin concentration from 0.5 to 2 U/mL. These results indicate that particle concentration (~8×10^6 particles/mL) was required to increase PA signal for heparin sensing. Particle concentration of each sample was measured using NTA technology. The error bars represent the standard deviation of five regions of interest.

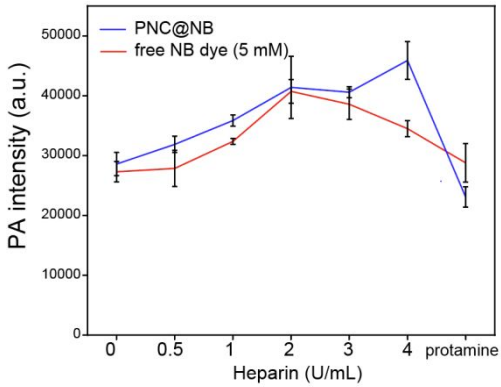

Figure S21. PA intensity comparison in whole human blood.
PA intensity of PNC@NB that loaded 80 μM of NB dye showed higher PA signal and had a broader therapeutic window than free NB dye with the concentration of 5 mM in whole human blood. The error bars represent the standard deviation of five regions of interest.

Figure S22. Photograph of PNC@NB-heparin interaction.
Photograph shows particle aggregation of PNC@NB after interacting with heparin concentration.

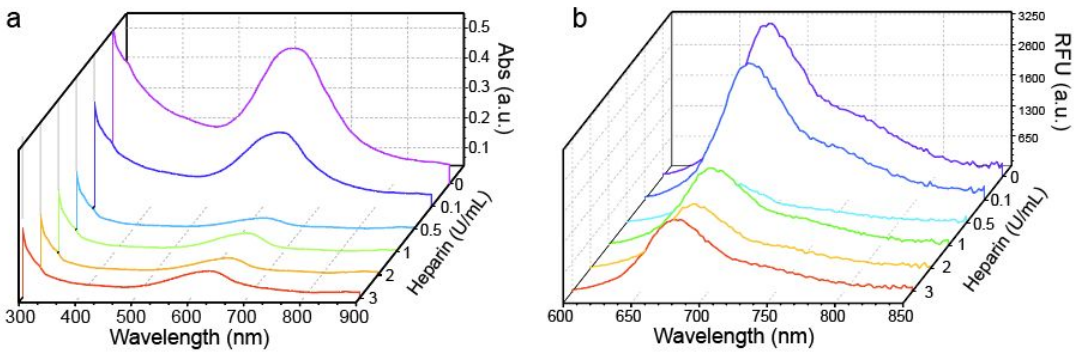

Figure S23. Decreased absorbance and fluorescence of PNC@NB.
Decrease in absorbance (**a**) and fluorescence (**b**) was observed after heparin interactions. The quenched fluorescence as a result of particle aggregation could lead to more PA signal.[6]

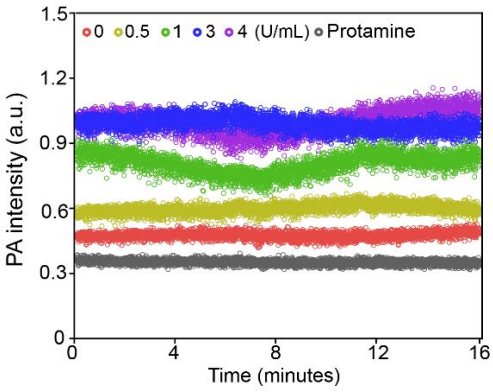

Figure S24. PA signal stability of PNC@NB.
PA signal generated from PNC@NB–heparin aggregation was stable for 15 min in whole human blood.

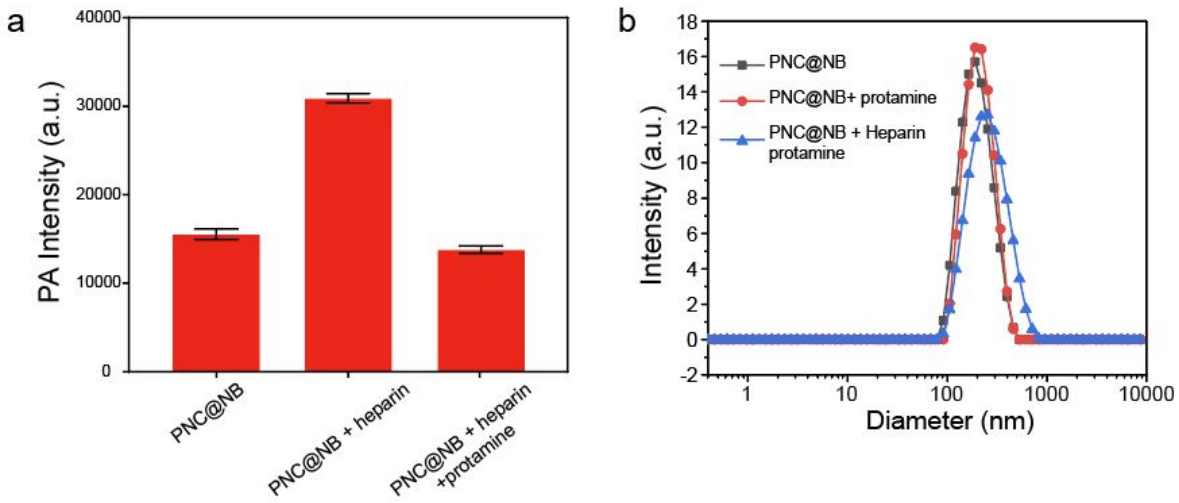

Figure S25. PA response of PNC@NB with/without protamine.
a In the presence of protamine, the increased PA signal of PNC@NB–heparin interaction turned off. Protamine is a positively charged heparin antagonist which can prevent interaction between heparin and PNC@NB. 1 U/mL of heparin and 80 μg of protamine were used for the reversal test.[7] The error bars represent the standard deviation of five regions of interest. **b** DLS data shows that there was no particle aggregation or disassembly of PNC@NB occurred in the presence of protamine.

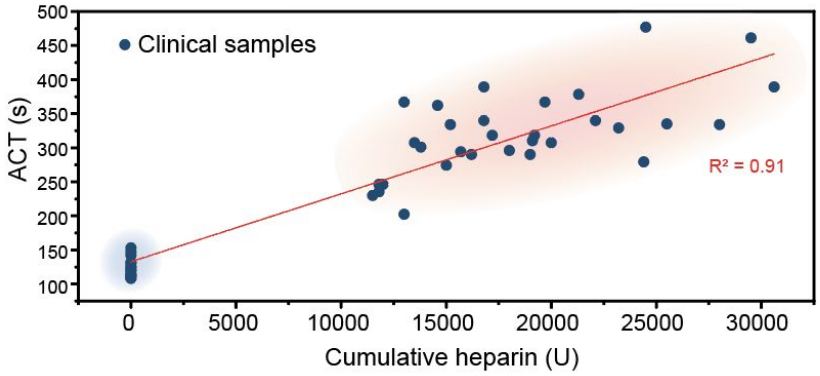

Figure S26. Linear correlation between ACT and cumulative heparin.
ACT values were linearly correlated with cumulative heparin ($R^2 = 0.91$). Clinical specimens were collected from 17 patients. Blue and red area indicate before (blue) and after (red) heparin infusion.

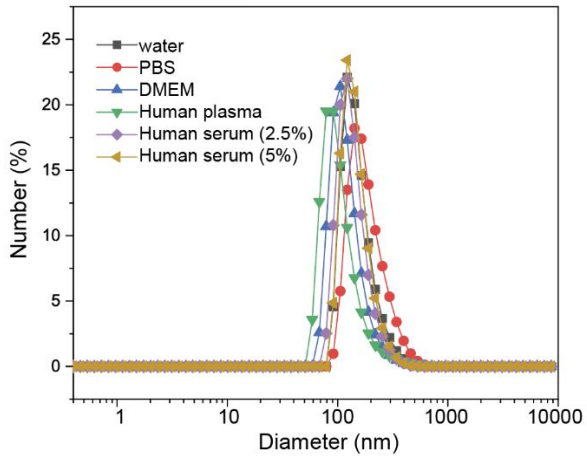

Figure S27. Colloidal stability of PNC@NB.
PNC@NB was incubated in different media (PBS, DMEM, human pooled plasma, 2.5% and 5% human serum) for 1 h, and showed negligible aggregation.

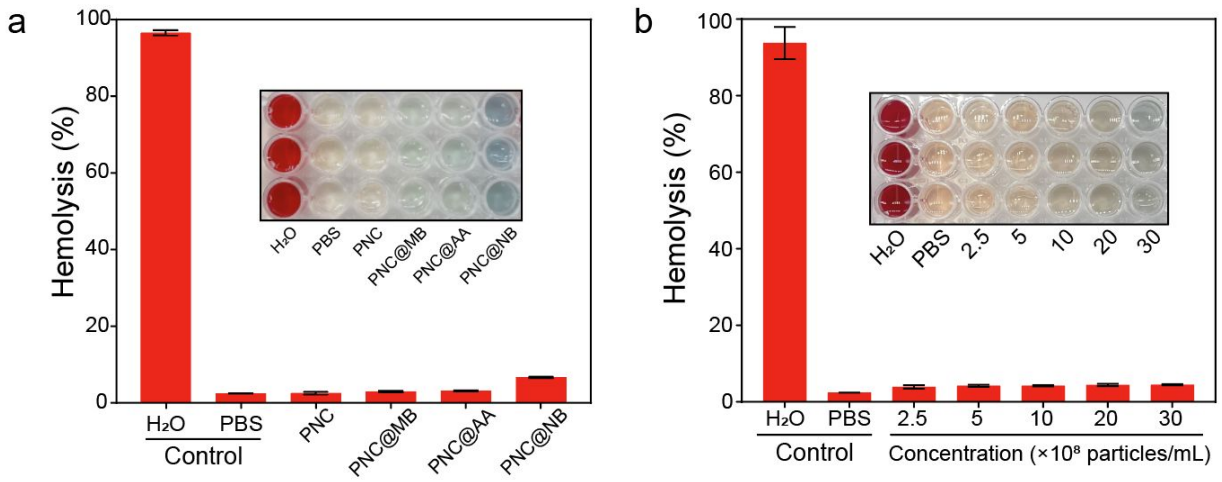

Figure S28. Hemolysis analysis of PNC, PNC@MB, PNC@AA, and PNC@NB.
a Hemolysis of PNC, PNC@MB, PNC@AA, and PNC@NB after incubation with red blood cells with the concentration of 30 $\times 10^8$ particles/mL used for heparin sensing. **b** Hemolysis of PNC@NB after incubation with red blood cells with the various concentrations (*e.g.,* 2.5 to 30 $\times 10^8$ particles/mL). PBS and deionized water were measured for negative and positive control. Inset image represent photograph of the solution supernatant after centrifugation at 4,000 *g* for 10 min. The error bars represent the standard deviation of three separate measurements.

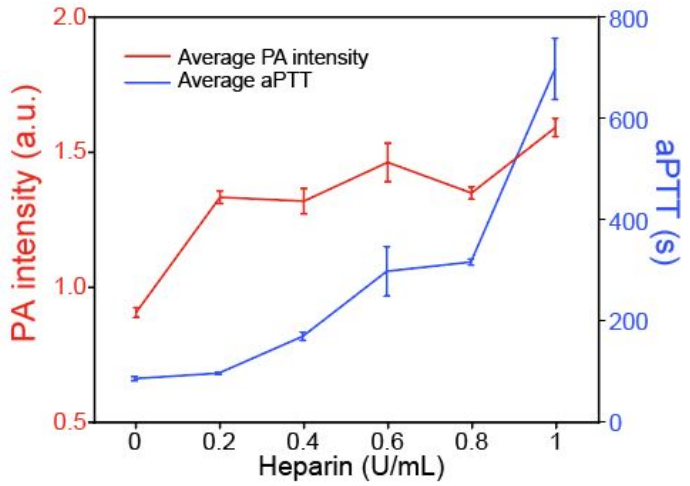

Figure S29. Correlation of aPTT and PA response of PNC@NB.
PA intensity of PNC@NB interacting with heparin concentration from 0.2 to 1 U/mL in human whole blood; the corresponding aPTT values were plotted against the heparin concentration. The error bars represent the standard deviation of three separate measurements.

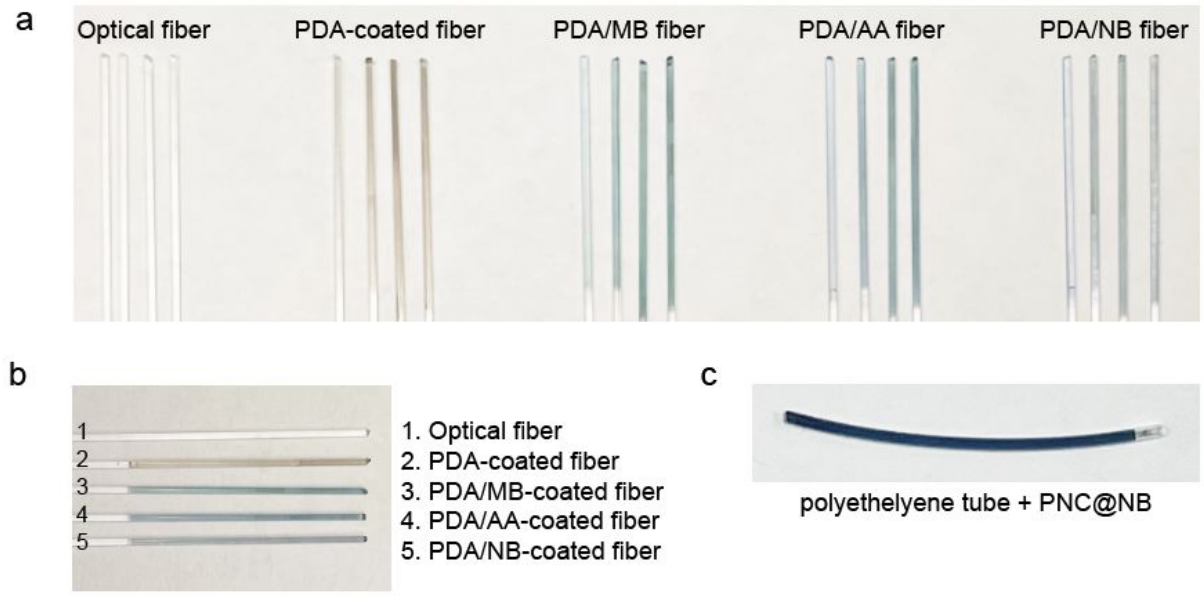

Figure S30. Proposed functional optic fiber for heparin detection.
a Taking advantage of adhesive nature of PDA, optical fibers were successfully coated with small molecular dyes (*e.g.,* MB, AA, and NB) with different dye concentration from low (left) to high (right). **b** Dye-coated optical fibers, enabled by PDA coating, and (**c**) PNC@NB-loaded polyethylene tube for future work for heparin detection *via* PA imaging.

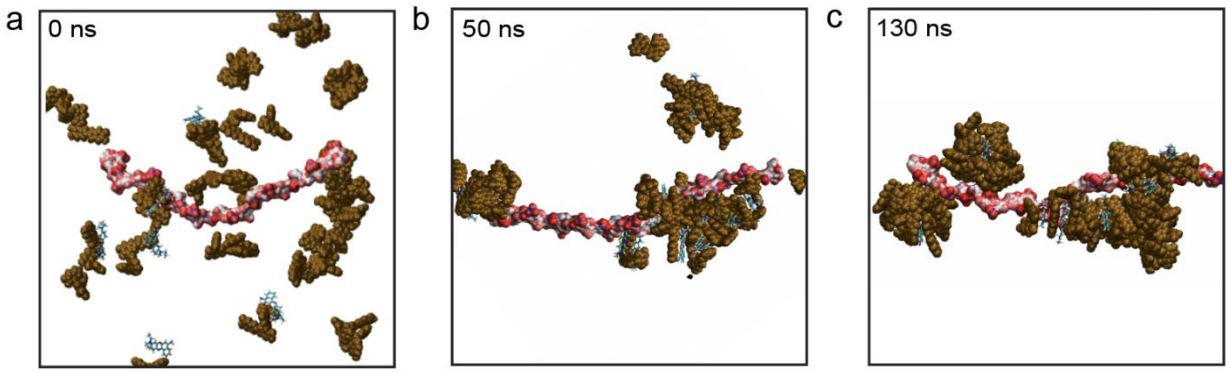

Figure S31. PDA–heparin interactions with NB dye.
MD simulation of interaction between PDA (brown) and heparin (red) in the presence of NB dyes at (**a**) 0 ns, (**b**) 50 ns, and (**c**) 130 ns. These results indicate that NB dyes bridged interaction between the PDA (brown) and heparin (red).

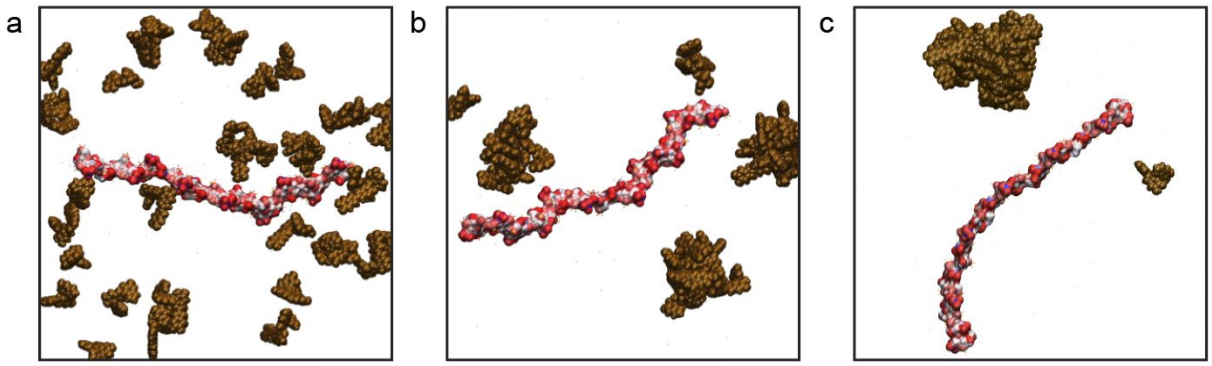

Figure S32. PDA–heparin interactions without NB dye.
MD simulation of interaction between PDA (brown) and heparin (red) at (**a**) 0 ns, (**b**) 50 ns, and (**c**) 130 ns. There was no observed particle aggregation when PDA alone interacted with heparin.

Table S1. PA imaging compared to other methods for monitoring heparin.

Method	Material	Turnaround time	Limit of detection (condition)	Therapeutic window	Clinical validation (y/n)	Clinical correlation (R^2)	Reference
Fluorescence imaging	silicon nanoparticle	15 min	0.004 U/mL (in PBS)	0.0044-0.44 U/mL (in PBS) 0.09-0.17 U/mL (in 50-fold diluted human serum)	y	n	[15]
	gold nanocluster	7 min	0.002 U/mL (in PBS)	0.02-0.35 U/mL (in PBS) 0.04-0.09 U/mL (in 50-fold diluted human serum)	y	n	[16]
	CuInS2 quantum dots	15 min	0.002 U/mL (in PBS)	0.04-1.1 U/mL (in PBS)	n	n	[17]
	graphene quantum dots	15 min	0.004 U/mL (in PBS)	0.02-0.35 U/mL (in PBS)	n	n	[18]
	mesoporous silica nanosphere	6 min	0.005 U/mL	0.01-2.2 U/mL	n	n	[19]
Colorimetric method	gold nanocluster	10 min	0.013 U/mL (in PBS)	0.02-0.66 U/mL (in PBS)	n	n	[21]
	gold nanoparticle	5 min	0.0003 U/mL (in water)	0.001-0.057 U/mL (in water) 0.001-0.005 U/mL (in diluted human serum)	y	n	[22]
	gold nanorod	15 min	0.002 U/mL (in HEPES buffer)	0.004-0.031U/mL (in HEPES buffer)	n	n	[23]
Electrochemical method	indium tin oxide	< 1 min	0.002 U/mL (in water)	0-0.04 U/mL (in water) 0-6 U/mL (in 100-fold diluted blood)	y	n	[24]
	methylene blue	< 1 min	0.06 U/mL (in water)	0.15-14.3 U/mL (in water)	n	n	[25]
	polyethyleneimine	5 min	0.066 U/mL (in PBS)	0.1-2 U/mL (in PBS) 1.6-83.2 U/mL (in 50-fold diluted rat serum)	n	n	[26]
Photoacoustic imaging	methylene blue	< 1 min	0.28 U/mL (in whole blood)	0.4-5 U/mL (in whole blood)	y	0.86 (1 patient)	[27]
	nile blue-coated cellulose	6 min	0.29 U/mL (in whole blood)	0.5-2.5 U/mL (in whole blood)	y	0.86 (16 patients)	[32]
	nile blue-coated nanocapsule (This study)	< 1 min	0.14 U/mL (in whole blood)	0.2-4 U/mL (in whole blood)	y	0.83 (17 patients)	

Clinical validation means that the methods validate with human samples.

REFERENCES

1. Armbruster, D. A.; Pry, T., Limit of Blank, Limit of Detection and Limit of Quantitation. *Clin. Biochem. Rev.* **2008,** *29* (Suppl 1), S49.
2. Schneider, C. A.; Rasband, W. S.; Eliceiri, K. W., NIH Image to ImageJ: 25 Years of Image Analysis. *Nat. methods* **2012,** *9* (7), 671-675.
3. McElfresh, C.; Harrington, T.; Vecchio, K. S., Application of a Novel New Multispectral Nanoparticle Tracking Technique. *Meas. Sci. Technol.* **2018,** *29* (6), 065002.
4. Zhou, J.; Lin, Z.; Penna, M.; Pan, S.; Ju, Y.; Li, S.; Han, Y.; Chen, J.; Lin, G.; Richardson, J. J., Particle Engineering Enabled by Polyphenol-Mediated Supramolecular Networks. *Nat. Commun.* **2020,** *11* (1), 1-8.
5. Liu, C.-Y.; Huang, C.-J., Functionalization of Polydopamine *via* the Aza-Michael Reaction for Antimicrobial Interfaces. *Langmuir* **2016,** *32* (19), 5019-5028.
6. Qin, H.; Zhou, T.; Yang, S.; Xing, D., Fluorescence Quenching Nanoprobes Dedicated to *in Vivo* Photoacoustic Imaging and High-Efficient Tumor Therapy in Deep-Seated Tissue. *Small* **2015,** *11* (22), 2675-2686.
7. Wang, J.; Chen, F.; Arconada-Alvarez, S. J.; Hartanto, J.; Yap, L.-P.; Park, R.; Wang, F.; Vorobyova, I.; Dagliyan, G.; Conti, P. S., A Nanoscale Tool for Photoacoustic-Based Measurements of Clotting Time and Therapeutic Drug Monitoring of Heparin. *Nano Lett.* **2016,** *16* (10), 6265-6271.
15. Ma, S.-d.; Chen, Y.-l.; Feng, J.; Liu, J.-j.; Zuo, X.-w.; Chen, X.-g., One-Step Synthesis of Water-Dispersible and Biocompatible Silicon Nanoparticles for Selective Heparin Sensing and Cell Imaging. *Anal. Chem.* **2016,** *88* (21), 10474-10481.
16. Li, S.; Huang, P.; Wu, F., Highly Selective and Sensitive Detection of Heparin Based on Competition-Modulated Assembly and Disassembly of Fluorescent Gold Nanoclusters. *New J. Chem.* **2017,** *41* (2), 717-723.
17. Liu, Z.; Ma, Q.; Wang, X.; Lin, Z.; Zhang, H.; Liu, L.; Su, X., A Novel Fluorescent Nanosensor for Detection of Heparin and Heparinase Based on CuInS2 Quantum Dots. *Biosen. Bioelectron.* **2014,** *54*, 617-622.
18. Li, Y.; Sun, H.; Shi, F.; Cai, N.; Lu, L.; Su, X., Multi-Positively Charged Dendrimeric Nanoparticles Induced Fluorescence Quenching of Graphene Quantum Dots for Heparin and Chondroitin Sulfate Detection. *Biosen. Bioelectron.* **2015,** *74*, 284-290.
19. Zhu, D.; Ye, J.; Hu, Y.; Wen, H. M.; Kang, A.; Tang, Y.-P.; Chen, J.; Shan, C. X.; Cui, X. B., Specific Enrichment Combined with Highly Efficient Solid-Phase Tagging for the Sensitive Detection of Heparin Based on Boronic Acid-Functionalized Mesoporous Silica Nanospheres. *Chem. Commun.* **2016,** *52* (79), 11779-11782.
20. Xu, M.; Wang, L. V., Photoacoustic Imaging in Biomedicine. *Rev. Sci. Instrum.* **2006,** *77* (4), 041101.
21. Hu, L.; Liao, H.; Feng, L.; Wang, M.; Fu, W., Accelerating the Peroxidase-Like Activity of Gold Nanoclusters at Neutral pH for Colorimetric Detection of Heparin and Heparinase Activity. *Anal. Chem.* **2018,** *90* (10), 6247-6252.
22. Qu, F.; Liu, Y.; Lao, H.; Wang, Y.; You, J., Colorimetric Detection of Heparin with High Sensitivity Based on the Aggregation of Gold Nanoparticles Induced by Polymer Nanoparticles. *New J. Chem.* **2017,** *41* (19), 10592-10597.
23. Bamrungsap, S.; Cherngsuwanwong, J.; Srisurat, P.; Chonirat, J.; Sangsing, N.; Wiriyachaiporn, N., Visual Colorimetric Sensing System Based on the Self-Assembly of Gold

Nanorods and Graphene Oxide for Heparin Detection Using a Polycationic Polymer as a Molecular Probe. *Anal. Methods* **2019,** *11* (10), 1387-1392.
24. Yoshimi, Y.; Sato, K.; Ohshima, M.; Piletska, E., Application of the 'Gate Effect'of a Molecularly Imprinted Polymer Grafted on an Electrode for the Real-Time Sensing of Heparin in Blood. *Analyst* **2013,** *138* (17), 5121-5128.
25. Tan, L.; Yao, S.; Xie, Q., Electrochemical Determination of Heparin Using Methylene Blue Probe and Study on Competition of Ba2+ with Methylene Blue for Binding Heparin. *Talanta* **2007,** *71* (2), 827-832.
26. Tian, L.; Zhao, H.; Zhao, Z.; Zhai, J.; Zhang, Z., A Facile Voltammetric Method for Detection of Heparin in Plasma Based on the Polyethylenimine Modified Electrode. *Anal. Methods* **2019,** *11* (10), 1324-1330.
27. Wang, J.; Chen, F.; Arconada-Alvarez, S. J.; Hartanto, J.; Yap, L.-P.; Park, R.; Wang, F.; Vorobyova, I.; Dagliyan, G.; Conti, P. S., A Nanoscale Tool for Photoacoustic-Based Measurements of Clotting Time and Therapeutic Drug Monitoring of Heparin. *Nano Lett.* **2016,** *16* (10), 6265-6271.
32. Jeevarathinam, A. S.; Pai, N.; Huang, K.; Hariri, A.; Wang, J.; Bai, Y.; Wang, L.; Hancock, T.; Keys, S.; Penny, W., A Cellulose-Based Photoacoustic Sensor to Measure Heparin Concentration and Activity in Human Blood Samples. *Biosens. Bioelectron.* **2019,** *126*, 831-837.

Descriptions for Supplementary Movie 1 and 2

Movie S1
Description: PDA–heparin interactions with NB dye.

Movie S2
Description: PDA–heparin interactions without NB dye.